Understanding the brittleness of metallic glasses through dynamic clusters

Wei-Dong Liu, Hai-Hui Ruan, and Liang-Chi Zhang[a)]
School of Mechanical and Manufacturing Engineering, University of New South Wales, Sydney 2052, Australia

(Received 12 July 2013; accepted 8 January 2014)

Exploiting molecular dynamics simulation, this article investigates the dynamic process of atomic rearrangement in two metallic glasses (MGs), $Cu_{50}Zr_{50}$ and $Fe_{80}P_{20}$, which are well known as ductile and brittle MGs under compression, respectively. It was found that the local rearrangements can be identified clearly by the distribution of kinetic energy and atomic strain rate, and that they are always driven by several high-velocity atoms in the core and induce a large shear and tensile strain over a very short duration. The size, kinetic energy, strain rate, and cavitation rate of the clusters in $Fe_{80}P_{20}$ are markedly larger than those in $Cu_{50}Zr_{50}$, which explains the distinct strength and brittleness of these two MGs. This study further confirmed that localized rearrangement of atomic structure is the underlying mechanism of plastic deformation in MGs, which governs their macro-scale mechanical performance.

I. INTRODUCTION

Metallic glasses (MGs) are newcomers of the time-honored alloy family.[1] They are generally fabricated by fast cooling from melt to maintain the structural disorder of the liquid state. Unlike traditional crystalline metals, the microstructure of a MG is completely amorphous, without any crystalline grain and long-range atomic periodicity.[2–4] As the metallic bond is much weaker than a covalent or an ionic bond, MGs possess the advantage of both glass and metal, demonstrated by their excellent electrical and thermal conductivities, much higher strength than their crystalline counterparts, and superplasticity under an elevated temperature.[5,6] However, the complicated mechanical behavior and the lack of ductility bottleneck the wide application of MGs. At room temperature, MGs are very brittle under tension but can become ductile under compression.[7] The strengths are insensitive to a large range of strain rates but reduce if the strain rate is beyond 10^3 s^{-1}.[8] In the supercooled liquid regime, however, MGs demonstrate superplasticity and rheological behavior with strong temperature and strain rate dependence.[7,9] It is also noted that the mechanical properties vary pronouncedly in different MG systems.[10,11] For example, Fe-based MGs possess much higher strength and much lower ductility than Zr-based MGs.[5] To understand these phenomena, a deep understanding of their atomistic deformation mechanism is necessary.

The plastic deformation of a MG is neither continuous nor homogenous,[12] which is manifested by the sudden bursts of plastic strain and shear banding.[9] Their microscopic picture is the localized atomic structural rearrangements, which occur stochastically and swiftly, causing the discrete plasticity events both temporarily and spaciously. From the energetic point of view, the atomic rearrangement can be considered as a process that the atomic system changes from one relatively low-energy configuration to another, crossing an activated configuration at the saddle.[13,14] At a high temperature, the thermal vibration is large enough to homogenously assist the crossover of configurations over the whole energy landscape, leading to the superplasticity of MG. At a low temperature, however, atomic rearrangements are biased toward the lowest saddle, inducing heterogeneous deformation and finally lead to shear banding failure.[15]

The atomic clusters undergoing rearrangement, which is named plastic unit in this article, are of certain size. Based on the classical theory of shear transformation zone (STZ),[16] it is generally regarded that the size of the STZ, on the order of hundreds (100–200) of atoms, is the characteristic size of a plastic unit. Therefore, the STZ theory or the subsequent development on cooperative shearing may be applied to quantify the size in an indirect way. Liu et al.[17] indirectly measured the average activation energy and the volume of plastic units of various MGs by a dynamic mechanical analysis (DMA). They found a correlation between the size of the flow units and the Poisson's ratio ν of the material. The MGs with a smaller sized plastic unit have larger values of ν and also better plasticity. Pan et al.[18] also evaluated the size of the plastic unit of various MGs through their strain rate sensitivity estimated by the instrumented nanoindentation, but obtained an opposite conclusion. Unlike the aggregated dislocations in crystalline metals, the plasticity events in

[a)]Address all correspondence to this author.
e-mail: Liangchi.Zhang@unsw.edu.au
DOI: 10.1557/jmr.2014.11

 © Materials Research Society 2014

https://doi.org/10.1557/jmr.2014.11 Published online by Cambridge University Press

MG do not leave any structural imprints for measuring them. The problem on the definition of these basic plastic units[19] has been poised by the inability in direct experimental characterization. Alternatively, molecular dynamics (MD) analysis has been used due to its simplicity in resolving the structural evolution and dynamics response.[20]

Chen and Ma.[21] studied the relationship between atomic structure and mechanical properties and concluded that plasticity events and shear banding are the results of the initial structural heterogeneity. Some structures, e.g., the icosahedra, are particularly stiff and hard to be rearranged.[21,22] The more are these structures, the less possible is shear banding. Shi and Falk[23] reported that shear band nucleates more easily in glasses produced at the lower cooling rate. Recent atomistic simulations of MGs indicated the length scale of plastic unit[24] based on the nanoscale density fluctuations, which are supposed to be the main cause of cavitation and brittle failure.[25,26] However, in these MD analyses, the nucleation of plastic units and their contributions to the deformation of bulk MG remains unclear.

This work uses the MD method to investigate two binary MGs of different ductility, $Zr_{50}Cu_{50}$ and $Fe_{80}P_{20}$, subjected to cryogenic deformation. Under such conditions, the effect of thermal fluctuation is minimized and the local atomic rearrangements can be discerned by the concomitant kinetic energy. This approach will allow us to identify the nucleation and evolution of plastic units, and hence to investigate the local strain rate and strain in these units and their influence on the global plastic deformation.

II. METHOD

The binary amorphous systems of $Cu_{50}Zr_{50}$ and $Fe_{80}P_{20}$ were constructed via a typical melt-quench process.[13,15] The many-body embedded atom potential was used to reflect the significance of the electron cloud for the metallic systems.[27,28] In the simulations, the pressure and temperature were kept constant through the Nose–Hover barostat and thermostat (updating every 0.2 ps), respectively. Periodic boundary conditions (PBC) in all directions were enforced. For both MGs, the initial atomic configurations were obtained by randomly distributing 20,000 atoms in a cube (6 nm $\times$ 12 nm $\times$ 6 nm). These models were then heated and equilibrated at 2000 K for 2 ns. The final specimens subjected to deformation were obtained through quenching the model to 0.1 K with the cooling rate of 100 K/ns. Uniaxial compression tests were performed by changing the height of the simulation box every 1 ps to achieve a strain rate of 7×10^8 s^{-1}. To compare the density and localization of shear band, big MG models of 400,000 atoms were also established by replicating the quenched small model for both MGs. Owing to the PBC, the replicating process does not induce interface mismatches.[29,30] In all MD simulations, the simulation time step is 2 fs.

The big models were subjected to simple shear under a shear strain rate of 5×10^8 s^{-1}. All MD simulations were conducted using the MD code, LAMMPS[31] and were analyzed with the aid of the open visualization tool, Ovitio.[32] Considering that the random atomic motion in the melt may lead to variation of amorphous structure after quenching, we repeated the simulation of the same material for at least three times. We also confirmed that increasing the sample size by even doubling the dimensions does not change the mechanical behavior.

III. RESULTS AND DISCUSSION

A. High kinetic energy clusters

The atoms involved in the plasticity event possess large translational kinetic energy (nonthermal components of kinetic energy) when the potential energy barrier that obstructs structural changes is overcome. This part of kinetic energy is hard to be distinguished at and beyond room temperature but becomes prominent at a sufficiently low temperature. Before loading, the maximum kinetic energies of the atoms in $Cu_{50}Zr_{50}$ and $Fe_{80}P_{20}$ induced by the thermal vibration are 1.1×10^{-4} and 1.2×10^{-4} eV, respectively. These two values are then set as the cut-off kinetic energies to distinguish fast atoms and slow atoms. In Fig. 1, the atoms with kinetic energy smaller than the cut-off value are removed. It is then noted that the remaining atoms form clusters, which can be considered as plastic units. These high kinetic energy clusters evaluated at every time step provide a direct way to trace the plasticity events in MG. In the $Cu_{50}Zr_{50}$ specimen, the clusters first emerging at the strain of 0.0154 are shown in Fig. 1(a). The average diameter of these clusters is about 1.5–2 nm, containing more than one hundred of atoms. It should be noted that this size is in line with the experimental results in Ref. 17, where the size of plastic unit was estimated from DMA experiments. In the $Fe_{80}P_{20}$ specimen, the clusters first appear at the strain of 0.035 with the size of 2–2.5 nm, which is larger than that in $Cu_{50}Zr_{50}$. This validates the experimental result that the material with lower ductility has relatively larger plastic units.[17] Along with the increasing strain, more and more clusters emerge and interact with each other, as shown in Fig. 1(c) for $Cu_{50}Zr_{50}$ and Fig. 1(d) for $Fe_{80}P_{20}$. But the follow-up phenomenon after the transitions occur is different in two MGs. In $Zr_{50}Cu_{50}$, the plastic units are smaller and more dispersed. On the contrary, the plastic units in $Fe_{80}Ni_{20}$ coalesce, which easily lead to catastrophic shear band failure (to be more elaborated in Sec. III. E).

In an equilibrium MD, the kinetic energy of atoms follows the same distribution regardless of the bond strength or particle mass. The cut-off kinetic energy we used is the maximum kinetic energy of particles identified in the isothermal relaxation. It can be regarded as a threshold arising from the equilibrium MD for pinpointing the

https://doi.org/10.1557/jmr.2014.11 Published online by Cambridge University Press

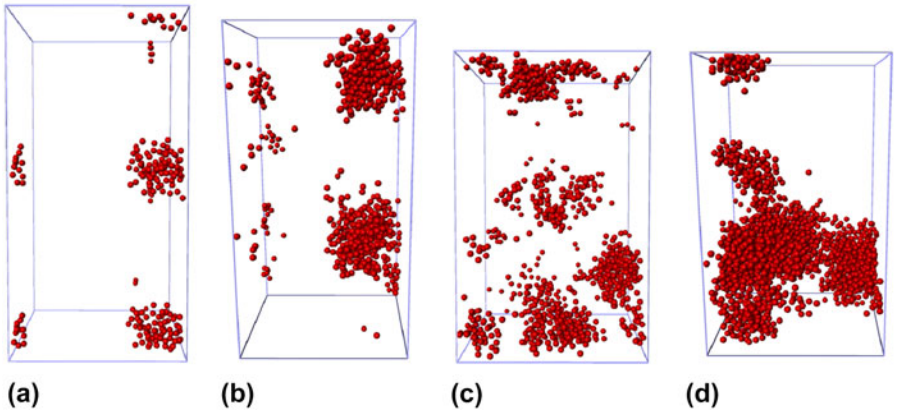


FIG. 1. The clusters of fast atoms in (a) $Zr_{50}Cu_{50}$ at strain 0.0154, (b) $Fe_{80}P_{20}$ at strain 0.035, (c) $Zr_{50}Cu_{50}$ at strain 0.14, and (d) $Fe_{80}P_{20}$ at strain 0.14.

effect of nonequilibrium dynamic process. The larger bond strength in Fe–P material system leads to more energy release when a barrier is crossed and affects a wider area. Therefore, it is rational to see that the rearranging cluster in $Fe_{80}P_{20}$ is larger than that in $Cu_{50}Zr_{50}$. It should be noted that we avoid calling them STZ because these clusters are the consequences of local rearrangement instead of the causes. Therefore, the size of the cluster does not directly indicate the size of STZ in a particular atomic system.

B. Variations of stress, potential energy, and kinetic energy

Figure 2(a) presents the uniaxial stress–strain curves of these two MGs. The general shapes of the two curves are very similar, including the initial elastic response, yielding, softening, and, finally, steady plastic flow. The elastic limit and yielding strength of both the MGs are much larger than those obtained in the experiment. The causes could be of 2-fold. First, the realistic samples unavoidably possess micro-scale imperfections such as surface notches, internal voids, micro-cracks, oxide inclusions, and nonmelted particles, where shear band nucleates more easily owing to stress concentration.[33] Second, the MD simulation uses an unrealistically high strain rate, which defers the inception of plasticity. It is noted that the first plastic clusters mentioned in Figs. 1(a) and 1(b) actually occur in the elastic regime. The bulk yielding point corresponds to the sudden surge of the number of clusters. After that, the continuous nucleation and annihilation of the clusters lead to the softening and a final steady flow stress. The total potential energies are shown in Fig. 2(b), in which the initial values are set to zero. One can find that the initial increase of potential energy in $Fe_{80}Ni_{20}$ is much steeper and larger than that in $Zr_{50}Cu_{50}$, making its yielding stress 2.5 times higher than that of $Zr_{50}Cu_{50}$. This ratio is in line with experimental results.[5] After yielding, the variation rates of the total potential energies reduce in the softening and steady plastic flow regime.

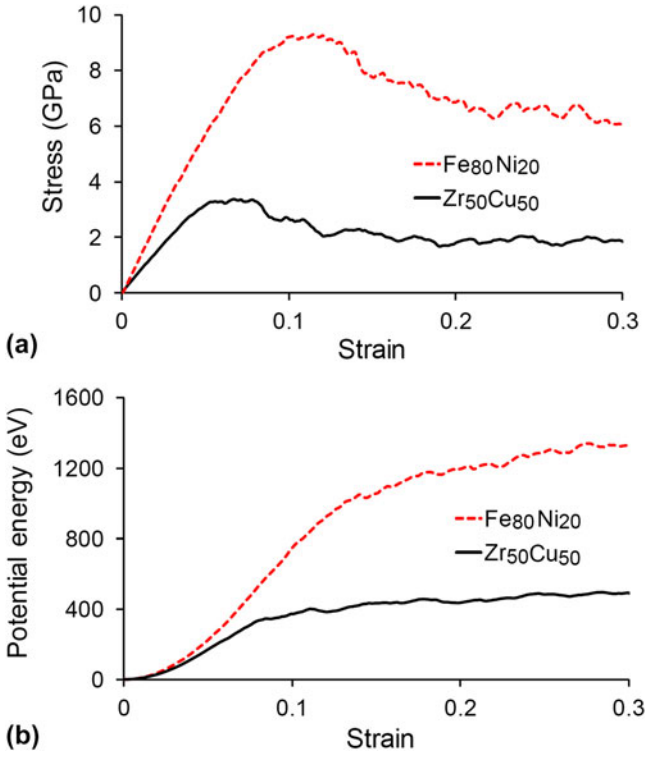


FIG. 2. The variation of stress (a) and potential energy (b) with the applied compressive strain for both $Zr_{50}Cu_{50}$ and $Fe_{80}P_{20}$ MGs.

The steady flow regime is a manifestation of the rise and fall of local potential energy in the plastic units, making the total potential energy levels off but the stress is nonzero. To elaborate this conception in detail, the variations of the average potential energies of Zr atoms in the clusters and in the whole specimen of $Zr_{50}Cu_{50}$ are calculated as shown in Fig. 3. The increase in the average potential energy of all Zr atoms approaches a plateau at large strain. However, the plastic clusters are in the activated state with much higher potential energy than the global average. Although continuous nucleation and

https://doi.org/10.1557/jmr.2014.11 Published online by Cambridge University Press

annihilation of the plastic units lead to the rise and fall of local potential energy (as indicated by the dashed line in Fig. 3), the average potential energy of the whole specimen remains at the position slightly higher than the minimum point, which therefore gives the nonzero stress. For comparison, the increase in the average potential energies of Fe atoms in the clusters and in the whole specimen of $Fe_{80}P_{20}$ is also shown, which exhibits the same phenomenon.

Figure 4 demonstrates the changes of average kinetic energy of atoms with strain of these two MGs, of which the peaks represent the nucleation and subsequent annihilation of plastic units. The small peaks of kinetic energy in the elastic regime indicate that the yielding point discerned from the stress–strain curve is not the incipient point of plastic deformation. Yielding actually indicates two phenomena: a relatively large peak induced by the formation of many plastic units and the stress level that activates the system and induces the continuous formation of many plastic units, manifested by many peaks in the curves of total kinetic energy.[13] It is noted that both the frequency and magnitude of the peaks in the kinetic energy curve of $Fe_{80}P_{20}$ are much larger than those of $Zr_{50}Cu_{50}$, corresponding to larger plastic units in $Fe_{80}P_{20}$ as shown in Fig. 1. The higher peak means that the atoms in rearrangement accumulate more potential energy due to a larger barrier. The higher frequency means that the nucleation and annihilation of plastic units in $Fe_{80}P_{20}$ are faster than those in $Zr_{50}Cu_{50}$.

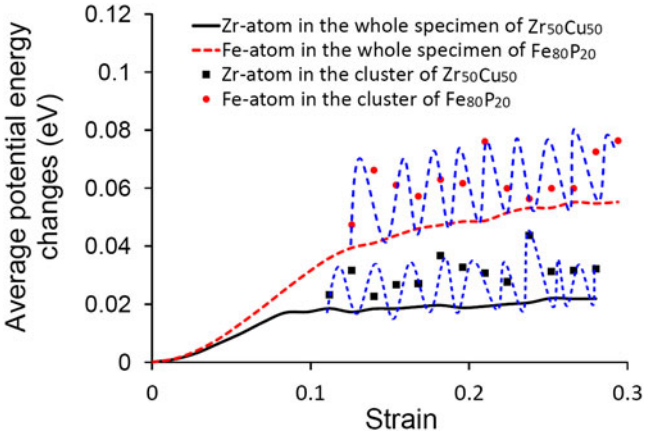


FIG. 3. The changes of the average potential energy: the black and red lines are the average potential energies of all Zr and Fe atoms in $Zr_{50}Cu_{50}$ and $Fe_{80}P_{20}$ specimens, respectively. The circles and squares represent, respectively, the average atomic potential energy of Zr-atom and Fe-atom in the rearranging clusters. They are calculated from a series of snapshots of instantaneous morphology. The blue dashed lines are the schematics of fluctuation (rise and fall) of potential energy within the cluster. They are the conception in understanding why the average potential energy in a cluster is notably larger than the global average one and the energetics of nucleation and disappearance of a rearranging cluster.

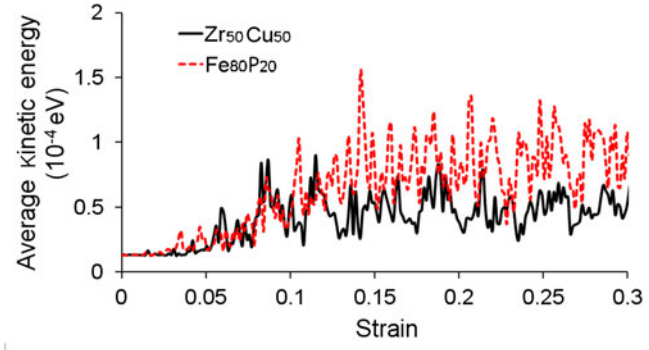


FIG. 4. The variation of the average kinetic energy with strain for both $Zr_{50}Cu_{50}$ and $Fe_{80}P_{20}$.

C. The distribution of kinetic energy

To understand the kinetics of these high kinetic energy clusters, we further analyze their details in the two MGs. Figure 5(a) shows the distribution of kinetic energy in a cluster of $Zr_{50}Cu_{50}$, in which the empty squares indicate the number of atoms with kinetic energy larger than the value indicated in the abscissa. The total number of atoms involved in the ZrCu cluster is 103, which is in line with the conception in theoretical and experimental works.[17,34] It is noted that there exists a large gradient of kinetic energy in the plastic unit. The core of the cluster is a Zr-atom and a Cu-atom with the kinetic energy of about 0.002 eV, an order of magnitude larger than that of other atoms in the cluster. It is conceived that the two atoms change their relative position swiftly causing the surrounding atomic structure to deform.[15] In the surrounding atoms, the distribution of kinetic energy can be fitted by the power law $P(E) \propto E^{-\beta}$ with $\beta = 1.43$. Compared with $Zr_{50}Cu_{50}$, the plastic unit of $Fe_{80}P_{20}$ involves more atoms (about 183) as shown in Fig. 5(b). The gradient of the kinetic energy in the $Fe_{80}P_{20}$ cluster is also much higher than that in $Zr_{50}Cu_{50}$. The maximum kinetic energy in the $Fe_{80}P_{20}$ cluster is almost 6 times larger than that of the $Zr_{50}Cu_{50}$ cluster and there are 8 atoms with the kinetic energy larger than 0.002 eV. Surrounding them, the distribution of kinetic energy in the rest of the atoms also follows the power law with a higher scaling factor $\beta = 1.48$. As aforementioned, the additional kinetic energy due to rearranging is owing to the potential energy barrier that is overcome. As the minima of the potential energy landscape (PEL) of $Fe_{80}P_{20}$ are much deeper than those in the PEL of $Zr_{50}Cu_{50}$, the resulting kinetic energy is much higher. However, both the $Zr_{50}Cu_{50}$ and $Fe_{80}P_{20}$ clusters share the same feature that the core of the plastic unit has several atoms with very large kinetic energy, which causes the reshuffling of the surrounding atomic structures.

Further information of atomic rearrangement can be obtained by investigating the distribution of kinetic energy in the whole specimen. In an equilibrium

https://doi.org/10.1557/jmr.2014.11 Published online by Cambridge University Press

isothermal system, the velocity distribution of atoms is Gaussian and the probability density function (PDF) of kinetic energy follows the χ^2-distribution:

$$f(E) = 2\sqrt{\frac{E}{\pi}}\left(\frac{1}{kT}\right)^{3/2}\exp\left[\frac{-E}{kT}\right] \quad , \qquad (1)$$

where k, T, and E are the Boltzmann constant, temperature, and kinetic energy of an atom, respectively. With Nose–Hover thermostat, the distribution of the kinetic energy in the MD system should follow this distribution. However, if the rearrangement occurs, the additional kinetic energy, induced by the release of the potential energy to the kinetic energy after crossing an energy barrier, leads to the bifurcation of PDF, as shown in Fig. 6(a) for the case of $Zr_{50}Cu_{50}$. Before a cluster nucleates, the PDF of kinetic energy follows the standard χ^2-distribution. When several clusters nucleate, the distribution of kinetic energy bifurcates from the χ^2-distribution to power-law distribution $f(E) \propto E^{-\alpha}$ with $\alpha = 1.96$. The kinetic energy distribution can return to the χ^2-distribution again after the rearrangement accomplishes since the additional heat is removed by the thermostat after some time. This is a process of local heat generation and dissipation due to the local rearrangement, indicating that the atomic rearrangement is dissipative. Similar bifurcation is also found in the case of $Fe_{80}P_{20}$ as shown in Fig. 6(b). Its scaling factor $\alpha = 2.77$ is larger than that of $Zr_{50}Cu_{50}$, corresponding to the larger gradient of kinetic energy in the plastic unit of $Fe_{80}P_{20}$. The power-law distribution is the signature of self-organized-criticality systems,[35] to which a MG at low temperature also belongs.[36] By comparing Fig. 6 with Fig. 5, it is clear that the bifurcation from the χ^2-distribution to power law is owing to the rearrangement of atoms in the plastic units. It should be noted that if the nucleation of plastic units is temporally and spaciously homogenous, the two scaling factors α and β should satisfy $\alpha - 1 = \beta$. Our results however deviate from this relation, which is probably caused by the dynamic heterogeneity.[12]

D. Strain and strain rate of clusters

To quantify the deformation rate of the clusters, we calculate atomic deformation rate $\mathbf{L}$ defined by

$$\mathbf{L}^i = \left(\sum_j \mathbf{d}^{ij} \otimes \left(\mathbf{v}^{ij}\right)^T\right) \cdot \left(\sum_j \mathbf{d}^{ij} \otimes \left(\mathbf{d}^{ij}\right)^T\right)^{-1}_{R_c} \quad , \qquad (2)$$

where $\mathbf{d}$ and $\mathbf{v}$ are the relative position and velocity vectors of the two atoms, respectively; superscripts i and j indicate the atom under consideration and the neighbor atom in the sphere of radius R_c centered at atom i, respectively; superscript T means transpose; and $\otimes$ is the dyadic

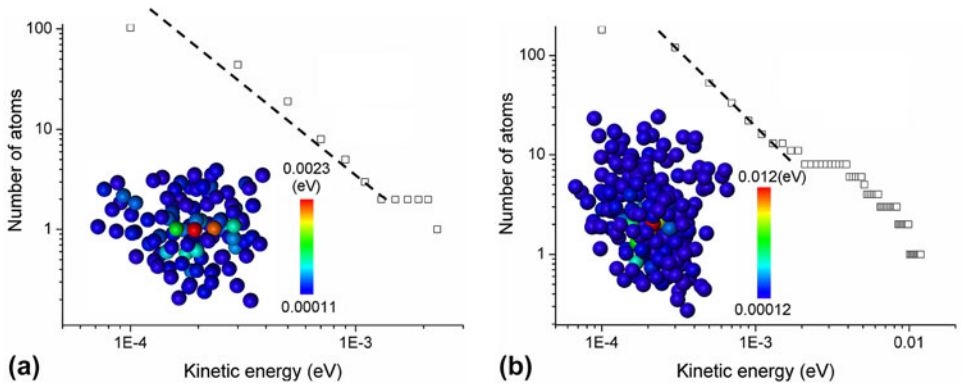


FIG. 5. Statistical distribution of the atomic kinetic energy and power-law fitting in (a) $Zr_{50}Cu_{50}$ and (b) $Fe_{80}P_{20}$ plastic units.

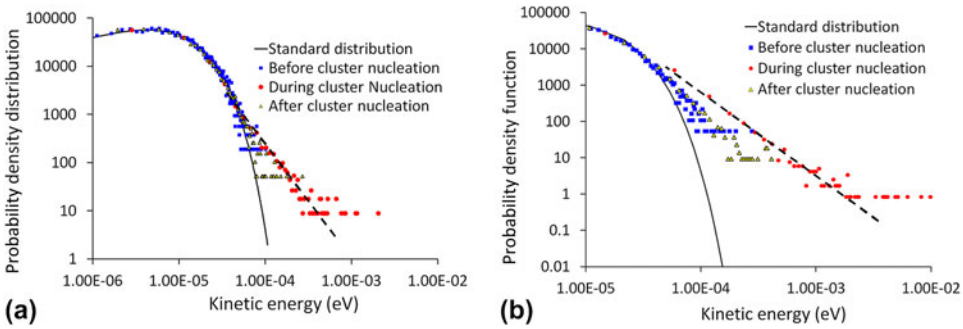


FIG. 6. PDFs of kinetic energy during the nucleation and dispersion of clusters in (a) $Zr_{50}Cu_{50}$ and (b) $Fe_{80}P_{20}$.

https://doi.org/10.1557/jmr.2014.11 Published online by Cambridge University Press

operator. The atomic strain rate tensor is then the symmetric part of $\mathbf{L}$, i.e.,$\dot{\boldsymbol{\varepsilon}} = \left(\mathbf{L} + \mathbf{L}^T\right)/2$. One can then compare the equivalent shear strain rate and volumetric strain rate for these two MGs. The distribution of the equivalent shear strain rate in $Zr_{50}Cu_{50}$ with the applied strain being 0.0154 is plotted in Fig. 7(a). It is noted that the high kinetic energy clusters are also high strain rate regions in which the maximum strain rate is about 200 times larger than the applied strain rate. In addition, the positive volumetric strain rate inside the plastic unit is also very large as shown in Fig. 7(b), indicating the significant local expansion. It is noted that both the maximum equivalent shear and volumetric strain rate in $Fe_{80}P_{20}$ are about 3 times larger than those in $Zr_{50}Cu_{50}$, as shown in Figs. 7(c) and 7(d), in accordance with the larger gradient of kinetic energy as seen in Fig. 5(b). The comparison of Figs. 7(b) and 7(d) leads to the conclusion that the cavitation rate in $Fe_{80}P_{20}$ is greater. Since the plastic unit is of a very brief lifetime, this rate difference does not necessarily lead to the conclusion that the probability of cavitation in $Fe_{80}P_{20}$ is more significant.

The atomic strain can also be calculated using OVITO[32] based on the formula proposed by Shimizu et al.[37] In the calculation, the reference configuration is that of the atomic system of 2 ps earlier than the current configuration, which leads to the strain increment in 2 ps. The local deformation gradient tensor F for each atom can be calculated from the relative displacements of the nearest neighbors within the given cut-off radius (0.5 nm). The Green–Lagrangian strain tensor is then obtained from the deformation gradient tensor F.[37] The equivalent shear strain and the volumetric strain were then calculated and plotted, as shown in Fig. 8. Similar to the distribution of strain rate, the atomic strain increment also concentrates inside some plastic units within 2 ps. The difference of the maximum equivalent shear strain increment between the two MGs is less significant than that of the maximum strain rate, owing to the shorter lifetime of the $Fe_{80}P_{20}$ plastic unit than that of the $Cu_{50}Zr_{50}$. However, the maximum volumetric expansion in $Fe_{80}P_{20}$ is still much greater than that in $Cu_{50}Zr_{50}$, indicating a larger probability of cavitation in $Fe_{80}P_{20}$.

E. Brittleness

Murali et al.[25] have reported the cavitation phenomena in the shear band under tensile stress in $Fe_{80}P_{20}$ and ascribed this to the cause of brittleness. Our results indicate that the tendency of cavitation is more significant in $Fe_{80}P_{20}$ than in $Zr_{50}Cu_{50}$, even under compression. Defining the ratio of the internal strain rate in the plastic unit to the applied strain rate as a measure of the local velocity disturbance owing to the atomic rearrangement. The larger disturbance renders the larger probability to

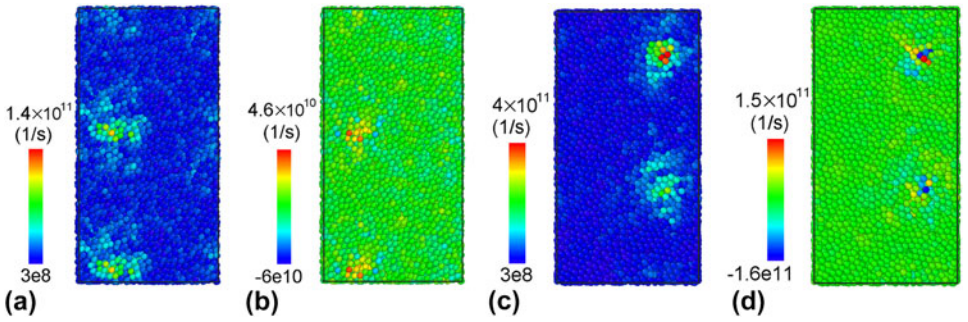


FIG. 7. Distributions of the equivalent shear strain rate in (a) $Zr_{50}Cu_{50}$ and (c) $Fe_{80}P_{20}$ and the volumetric strain rate in (b) $Zr_{50}Cu_{50}$ and (d) $Fe_{80}P_{20}$. In these figures, the applied compressive strains are 0.0154 for $Zr_{50}Cu_{50}$ and 0.035 for $Fe_{80}P_{20}$.

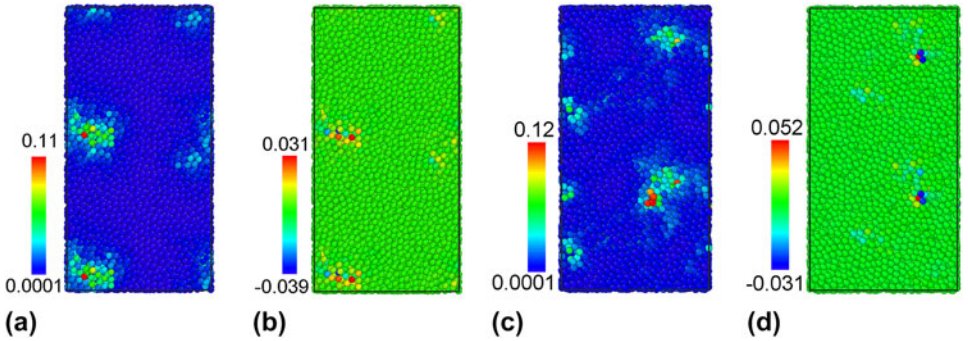


FIG. 8. Distributions of the equivalent shear strain increment in (a) $Zr_{50}Cu_{50}$ and (c) $Fe_{80}P_{20}$ and the volumetric strain increment in (b) $Zr_{50}Cu_{50}$ and (d) $Fe_{80}P_{20}$. In these figures, the applied compressive strains are 0.0154 for $Zr_{50}Cu_{50}$ and 0.035 for $Fe_{80}P_{20}$.

https://doi.org/10.1557/jmr.2014.11 Published online by Cambridge University Press

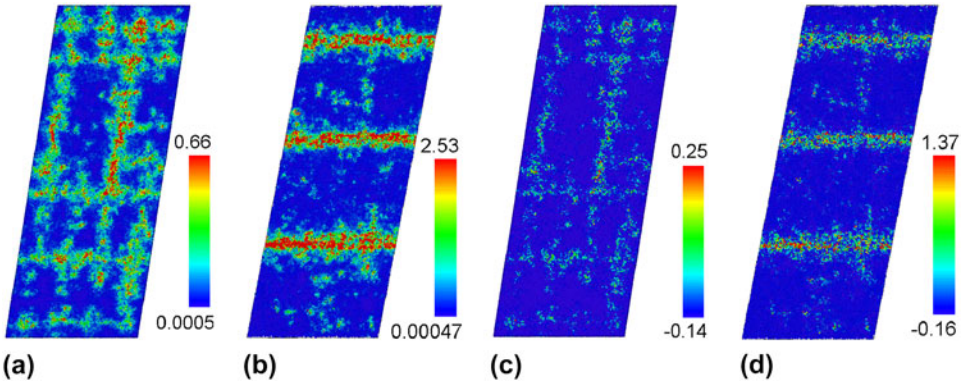


FIG. 9. Distributions of the equivalent shear strain increment in (a) $Zr_{50}Cu_{50}$ and (b) $Fe_{80}P_{20}$ and the volumetric strain increment in (c) $Zr_{50}Cu_{50}$ and (d) $Fe_{80}P_{20}$. In these figures, the applied shear strains are 0.15 for $Zr_{50}Cu_{50}$ and 0.2 for $Fe_{80}P_{20}$. The difference is owing to the difference in their elastic limits as indicated in Fig. 2(a), which is about 0.05 for the simple shear case.

induce the nucleation and unstable propagation of a shear band.[15] This accounts why $Fe_{80}P_{20}$ is more brittle than $Zr_{50}Cu_{50}$. First, the dynamic local rearrangement induces more significant disturbance in the velocity field, causing the more probability in triggering the propagation of shear bands. Second, the rearrangement-induced cavitation is more significant in $Fe_{80}P_{20}$, causing more alleviation of atoms (or inducing more free volume) in the shear bands.

For a further verification, a simple shear of larger atomic models (6 nm × 24 nm × 60 nm) is simulated for both the MGs. Figure 9(a) exhibits the increment of equivalent shear strain in $Zr_{50}Cu_{50}$ at the applied shear strain of 0.15. The reference is the configuration of the atomic system 30 ps earlier than the current configuration. It is noted that the plastic deformation is localized in some bands. These bands are the precursors of major shear band since they do not run across the sample. However, in $Fe_{80}P_{20}$, the catastrophic shear bands with the larger shear strain over the same 30 ps have formed as shown in Fig. 9(b). Figures 9(c) and 9(d) compare the volumetric strain distribution in both materials. It is striking that the cavitation in $Fe_{80}P_{20}$ is much more significant and is well within the catastrophic shear bands.

IV. CONCLUSIONS

In this paper, we have characterized the plastic unit of MG with the aid of MD analysis for two typical MGs: $Cu_{50}Zr_{50}$, which is macroscopically ductile in compression and $Fe_{80}P_{20}$, which is brittle. Our simulation results indicate that the size of the plastic unit of the brittle MG, $Fe_{80}P_{20}$, is much larger than that in $Cu_{50}Zr_{50}$. This is due to the deeper minimum in the PEL of $Fe_{80}P_{20}$ and the larger strain rate in the plastic unit. Shear banding can be more easily triggered in $Fe_{80}P_{20}$, and the subsequent larger cavitation inside shear bands leads to larger brittleness. By investigating the dynamics of atoms in plastic units, this work underpins the fundamental cause of the large variation of ductility of MGs.

Last, it is necessary to point out that MD simulation is rather unrealistic since the cooling rates and the strain rates are unrealistically high and the Nose–Hoover thermostat does not resolve the thermal conduction, particularly electronic conduction, in MG. These effects are hard to assess. Thus, the kinetic energy associated with a rearranging cluster as well as the local strain rate is only meaningful for a qualitative understanding of the mechanisms and should not be considered as realistic scenarios.

ACKNOWLEDGMENTS

The authors appreciate the Australian Research Council for its financial support to this work. This work was also supported by an award under the Merit Allocation Scheme on the NCI National Facility at ANU and computational resources provided by Intersect Australia Ltd.

REFERENCES

1. C.S.A. Inoue: *Bulk Metallic Glasses* (CRC Press, Boca Raton, FL, 2011).
2. A.L. Greer, K.L. Rutherford, and M. Hutchings: Wear resistance of amorphous alloys and related materials. *Int. Mater. Rev.* **47**(2), 87 (2002).
3. W.L. Johnson: Bulk amorphous metal: An emerging engineering material. *JOM* **54**(3), 40 (2002).
4. W.H. Wang, X.Q. Zang, and R.S. Lu: Low formaldehyde emission particleboard bonded by UF-MDI mixture adhesive. *For. Prod. J.* **54**(9), 36 (2004).
5. M.W. Chen: Mechanical behavior of metallic glasses: Microscopic understanding of strength and ductility. *Annu. Rev. Mater. Res.* **38**, 445 (2008).
6. A. Inoue: Stabilization of metallic supercooled liquid and bulk amorphous alloys. *Acta Mater.* **48**(1), 279 (2000).
7. J. Lu, G. Ravichandran, and W.L. Johnson: Deformation behavior of the $Zr_{41.2}Ti_{13.8}Cu_{12.5}Ni_{10}Be_{22.5}$ bulk metallic glass over a wide range of strain-rates and temperatures. *Acta Mater.* **51**(12), 3429 (2003).
8. W.D. Liu, K.X. Liu, X.X. Xia, and W.H. Wang: The failure stress of bulk metallic glasses under very high strain rate. *J. Mater. Res.* **25** (7), 1230 (2010).

https://doi.org/10.1557/jmr.2014.11 Published online by Cambridge University Press

9. C.A. Schuh, T.C. Hufnagel, and U. Ramamurty: Overview No. 144 – Mechanical behavior of amorphous alloys. *Acta Mater.* **55**(12), 4067 (2007).
10. G. Wang, D.Q. Zhao, H.Y. Bai, M.X. Pan, A.L. Xia, B.S. Han, X.K. Xi, Y. Wu, and W.H. Wang: Nanoscale periodic morphologies on the fracture surface of brittle metallic glasses. *Phys. Rev. Lett.* **98**(23), 235501 (2007).
11. J. Schroers and W.L. Johnson: Ductile bulk metallic glass. *Phys. Rev. Lett.* **93**(25), 255506 (2004).
12. D. Rodney, A. Tanguy, and D. Vandembroucq: Modeling the mechanics of amorphous solids at different length scale and time scale. *Modell. Simul. Mater. Sci. Eng.* **19**(8), 083001 (2011).
13. W.D. Liu, H.H. Ruan, and L.C. Zhang: On the plasticity event in metallic glass. *Philos. Mag. Lett.* **535–536**, 158 (2013).
14. H.H. Ruan, L.C. Zhang, and J. Lu: A new constitutive model for shear banding instability in metallic glass. *Int. J. Solids Struct.* **48** (21), 3112 (2011).
15. W.D. Liu, H.H. Ruan, and L.C. Zhang: Atomic rearrangements in metallic glass: Their nucleation and self-organization. *Acta Mater.* **61**(16), 6050 (2013).
16. A.S. Argon: Plastic-deformation in metallic glasses. *Acta Metall. Mater.* **27**(1), 47 (1979).
17. S.T. Liu, Z. Wang, H.L. Peng, H.B. Yu, and W.H. Wang: The activation energy and volume of flow units of metallic glasses. *Scr. Mater.* **67**(1), 9 (2012).
18. D. Pan, A. Inoue, T. Sakurai, and M.W. Chen: Experimental characterization of shear transformation zones for plastic flow of bulk metallic glasses. *Proc. Natl. Acad. Sci. U.S.A.* **105**(39), 14769 (2008).
19. R. Dasgupta, S. Karmakar, and I. Procaccia: Universality of the plastic instability in strained amorphous solids. *Phys. Rev. Lett.* **108** (7), 075701 (2012).
20. S. Takeuchi and K. Edagawa: Atomistic simulation and modeling of localized shear deformation in metallic glasses. *Prog. Mater. Sci.* **56**(6), 785 (2011).
21. Y.Q. Cheng and E. Ma: Atomic-level structure and structure-property relationship in metallic glasses. *Prog. Mater. Sci.* **56**(4), 379 (2011).
22. A.J. Cao, Y.Q. Cheng, and E. Ma: Structural processes that initiate shear localization in metallic glass. *Acta Mater.* **57**(17), 5146 (2009).
23. Y.F. Shi and M.L. Falk: Strain localization and percolation of stable structure in amorphous solids. *Phys. Rev. Lett.* **95**(9), 095502 (2005).
24. P. Murali, Y.W. Zhang, and H.J. Gao: On the characteristic length scales associated with plastic deformation in metallic glasses. *Appl. Phys. Lett.* **100**(20), 201901 (2012).
25. P. Murali, R. Narasimhan, T.F. Guo, Y.W. Zhang, and H.J. Gao: Shear bands mediate cavitation in brittle metallic glasses. *Scr. Mater.* **68**(8), 567 (2013).
26. P. Murali, T.F. Guo, Y.W. Zhang, R. Narasimhan, Y. Li, and H.J. Gao: Atomic scale fluctuations govern brittle fracture and cavitation behavior in metallic glasses. *Phys. Rev. Lett.* **107**(21), 215501 (2011).
27. G.J. Ackland, M.I. Mendelev, D.J. Srolovitz, S. Han, and A.V. Barashev: Development of an interatomic potential for phosphorus impurities in alpha-iron. *J. Phys. Condens. Matter* **16**(27), S2629 (2004).
28. M.I. Mendelev, M.J. Kramer, R.T. Ott, D.J. Sordelet, D. Yagodin, and P. Popel: Development of suitable interatomic potentials for simulation of liquid and amorphous Cu-Zr alloys. *Philos. Mag.* **89**(11), 967 (2009).
29. T. Schlick: *Molecular Modeling and Simulation: An Interdisciplinary Guide* (Springer, New York, NY, 2002).
30. D.C. Rapaport: *The Art of Molecular Dynamics Simulation* (Cambridge University Press, New York, NY, 2004).
31. S. Plimpton: Fast parallel algorithms for short-range molecular-dynamics. *J. Comput. Phys.* **117**(1), 1 (1995).
32. A. Stukowski: Visualization and analysis of atomistic simulation data with OVITO-the Open Visualization Tool. *Modell. Simul. Mater. Sci. Eng.* **18**(1), 015012 (2010).
33. Y.Q. Cheng and E. Ma: Intrinsic shear strength of metallic glass. *Acta Mater.* **59**(4), 1800 (2011).
34. W.L. Johnson and K. Samwer: A universal criterion for plastic yielding of metallic glasses with a (T/Tg)(2/3) temperature dependence. *Phys. Rev. Lett.* **95**(19), 195501 (2005).
35. P. Bak, C. Tang, and K. Wiesenfeld: Self-organized criticality: An explanation of 1/F noise. *Phys. Rev. Lett.* **59**(4), 381 (1987).
36. B.A. Sun, H.B. Yu, W. Jiao, H.Y. Bai, D.Q. Zhao, and W.H. Wang: Plasticity of ductile metallic glasses: A self-organized critical state. *Phys. Rev. Lett.* **105**(3), 035501 (2010).
37. F. Shimizu, S. Ogata, and J. Li: Theory of shear banding in metallic glasses and molecular dynamics calculations. *Mater. Trans.* **48**(11), 2923 (2007).

https://doi.org/10.1557/jmr.2014.11 Published online by Cambridge University Press